Comparative study on the effect of (Cr, Mo, V)-alloying on transformation and mechanical behavior of 0.2 wt.% C TRIP-assisted steel

Roman A. Kussa[1], Vadym I. Zurnadzhy[1], Manuele Dabala[2], Mattia Franceschi[2],
Vasily G. Efremenko[1]*, Ivan Petryshynets[3], František Kromka[3], Michail N. Brykov[4]

[1]*Pryazovskyi State Technical University, Mariupol 87555, Ukraine*
[2]*University of Padova, Padova 35131, Italy*
[3]*Institute of Materials Research, Slovak Academy of Sciences, Košice 04001, Slovak Republic*
[4]*Zaporizhzhia Polytechnic National University, Zaporizhzhia 69063, Ukraine*

Abstract

The structure and mechanical properties of two 0.2 wt.% C TRIP-assisted steels (Transformation Induced Plasticity) were compared to evaluate the effect of additional (Cr, Mo, V)-alloying on transformation kinetic and tensile/impact behavior after isothermal bainite transformation (bainitizing) and Q&P (Quenching-and-Partitioning) treatment. The work was performed using SEM, XRD, tensile/impact testing, and computer simulation. It was found that adding 0.55 wt.% Cr, 0.2 wt.% Mo, and 0.11 wt.% V into Mn-Si-Nb steel increased the incubation time in pearlite and bainite temperature ranges by 5.6 and 4.4 times, respectively. More heavily alloyed steel performed an improved combination "Strength/Ductility/Impact Toughness": its maximum PSE (Product of Strength and Elongation) value of 24 GPa·% referred to bainitizing treatment, whereas the highest $KCV_{20°C}$ values (220–225 J cm^{-2}) corresponded to Q&P treatment. Improved mechanical properties of (Cr, Mo, V)-alloyed steel were attributed to a higher amount of retained austenite and a slower rate of TRIP-effect.

K e y   w o r d s: TRIP-assisted steel, bainitizing, Q&P, austenite, mechanical properties

1. Introduction

TRIP-assisted (TRIP-aided) steels belong to the first generation of advanced high-strength steels (AHSSs) intended for applications in automotive, construction, infrastructure industries, performing an ultimate strength higher than 550 MPa [1, 2]. An improved steel strength (tensile strength of 600–1100 MPa [3]) allows reducing construction weight which is of great cost-saving and environmental-friendly importance [3, 4]. TRIP-assisted steels are low-alloyed compositions with a multiphase microstructure comprising ferrite, bainite, and retained austenite (RA), whereas RA volume fraction is up to 10–15 vol.% [5, 6]. This is due to a specific alloying, which includes the increased amount of silicon (aluminum) to suppress the carbide precipitation during the phase transformation [7–9]. Carbon-rich austenite performs higher stability under the bainitizing holding or undercooling, thus enabling its retention in the structure. Retained austenite exhibits the tendency for strain-induced martensite transformation (SIMT), thus providing TRIP-effect [10, 11]. It is generally recognized that RA and TRIP-effect are responsible for improved mechanical [12, 13] and exploitation [14, 15] performance of steels and cast irons. Ductile austenite improves the steel ability for strain flow, while SIMT contributes to work hardening and ductility (the latter is due to delaying the neck formation [16]). Also, TRIP-effect is considered as a stress relaxation mechanism inhibiting the crack nucleation and propagation [17, 18]. Summing up, TRIP-effect is an effective approach to increase strength/ductility complex that is beneficial for steels behavior under its processing and exploitation.

The multiphase state of TRIP-assisted steels can

Table 1. Chemical composition of the steels studied

Steel designation	Composition (wt.%)									
	C	Si	Mn	Cr	Mo	V	Nb	S	P	Fe
A	0.18	1.50	1.80	–	–	–	0.055	0.010	0.010	Bal.
B	0.20	1.79	1.73	0.55	0.20	0.11	0.045	0.009	0.013	Bal.

be acquired by using different approaches. The main ones are bainitizing processing [18, 19] and Q&P-treatment [20, 21]. Bainitizing aims at "austenite → bainite" transformation to get the microstructure of low bainite or carbide-free nanostructured bainite (which is essentially the nanosized ferritic laths and film-like retained austenite) [22, 23]. The nanobainite concept proposed by Bhadeshia et al. [24] for high-carbon steels has been further transferred to lower carbon steels [25]. Q&P (quenching-and-partitioning) includes interrupted quenching to form some portion of fresh martensite. The subsequent holding at quenching temperature (one-step partitioning) or higher temperature (two-step partitioning) promotes the carbon diffusion from martensite to austenite leading to its stabilization (retaining in the structure) through the carbon enrichment [26–28]. Also, bainite transformation may occur during the partitioning contributing to austenite stabilization through the carbon diffusion from bainitic ferrite. Due to pre-formed martensite, Q&P-treated steels have a higher tensile strength/hardness that may broaden their application for tool and heavily-load machinery products [26, 29]. Both approaches effectively promote an austenite carbon enrichment, ensuring a higher RA volume fraction.

TRIP-assisted steels and Q&P-steels are similar in their chemical composition. They both are low-alloyed in order to meet the cost-effectiveness requirements. They are alloyed mainly by Mn and Si (Al) (up to 3 wt.% each) with a lower amount of Cr, Mo, Ni, etc. [26, 28, 29]. The strong carbide-forming elements (V, Nb, Ti) may also be micro-added to TRIP-steels, improving the mechanical properties due to precipitation strengthening mechanism under TMCP (Thermo-Mechanical Controlled Process) or heat processing [30–32]. However, even a small addiction of expensive alloying elements negatively affects the cost of TRIP-steel; therefore, their adding must be justified in terms of the corresponding enhancement of properties. With this regard, systematic studies on "composition–properties" correlations are required in order to optimize the TRIP-assisted steel chemical composition. This research effort aimed to compare the tensile/impact behavior of two low-carbon steels, which fall into the TRIP-assisted concept, slightly differing in strong carbide-forming elements (Cr, Mo, V) concentrations.
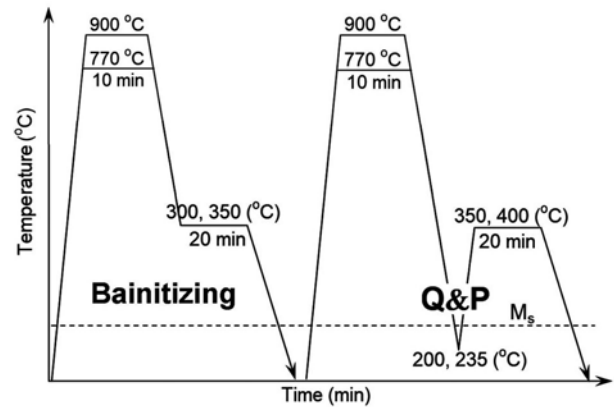

Fig. 1. The scheme of heat treatment of the steels.

2. Methods

The studied materials were steels A and B with a chemical composition presented in Table 1. Steels were melted in a 120-kg induction furnace using the pig iron, steel scrap, and master-alloys (FeSi, FeMn, FeCr, FeMo, FeNb, FeV). Both steels were similar by C, Mn, Si, Nb contents, while steel B was additionally alloyed with Cr, Mo, and V to improve its hardenability and mechanical properties. The ingots of 50 mm diameter and 300 mm length were obtained by pouring the melt into the graphite molds. The ingots were then welded to a single long electrode which afterward was electro-slag remelted to produce an 80 mm diameter ingot. The final ingot was austenized at 1150 ℃ for subsequent forging and rolling to a 15 mm thick strip. The strip was used to machine the specimens for tensile/impact testing and microstructure characterization. Before machining, the strip was softened by annealing at 950 ℃ and slow cooling to room temperature. Tensile specimens were of 5 mm diameter and 30 mm long gauge; the V-notched impact specimens were 55 long and $7.5 \times 10\,\text{mm}^2$ in cross-section.

The specimens were subjected to heat treatments according to different schemes, namely bainitizing and Q&P (Fig. 1). Each scheme included the 10-min heating at austenitization temperature (t_A) of 770 ℃ or 900 ℃. The bainitizing scheme included the subsequent keeping of austenized specimens in (60 wt.% Sn + 40 wt.% Pb)-bath for 20 min at bainite transformation temperature (t_B) of 300 or 350 ℃ with fur-

ther air-cooling. Under Q&P scheme, the heated specimens were quenched in Wood's metal alloy bath to 235 °C (t_A = 900 °C) or 200 °C (t_A = 770 °C). The bath temperature (t_Q) was below Ms temperature being selected in order to obtain the maximal amount of retained austenite, according to the procedure reported by Clarke et al. [33]. After the holding for 1 min in quenching bath, the specimens were partitioned in (60 wt.% Sn + 40 wt.% Pb)-bath for 20 mm at the partitioning temperature (t_P) of 350 or 400 °C and cooled in still air. The heat treatment regimes are designated in the text as "t_A-t_B" (bainitizing) and "t_A-t_Q-t_P" (Q&P treatment).

Mechanical testing was performed using UIT STM 100S universal servo-driven tensile testing machine (UKRINTECH) and Charpy impact testing machine. The tensile and impact tests were conducted at room temperature and 60–70 vol.% air humidity. The microstructure was studied on the mirror-polished specimens after etching with 4 vol.% nitric acid-alcohol solution. An optical microscope (OM) Axiovert 40 MAT (Carl Zeiss) and a scanning microscope EVO MA15 (Carl Zeiss) were used for the microstructure characterization.

The phase constituents of the steels were revealed by an X'Pert PRO diffractometer (PANalytical) using Cu-Kα radiation under the following parameters: voltage is 40 kV, the tube current is 50 mA, the scan step is 0.033 degrees, the scan speed is 0.069 degree s^{-1}. The phase transformation kinetic was simulated using JMatPro software.

The phase constituents were identified using XRD using diffractometer D8 Da Vinchi Brucker with Cu-Kα radiation. The volume fraction of retained austenite (VF_{RA}) was calculated using Eq. (1):

$$VF_{RA} = \frac{100\%}{1 + G(I_\alpha/I_\gamma)}, \qquad (1)$$

where I_α and I_γ are integrated intensities of diffraction peaks of ferrite (200), (211) and austenite (200), (220), (311); G is the fitting coefficient for different peaks combinations [34]. The volume fraction of RA was an average of the VF_{RA} values calculated for different pairs of lines.

The concentration of carbon in retained austenite (C_{RA}) was derived from the Eq. (2):

$$\alpha_\gamma = 0.3556 + 0.0453[C_{RA}] + 0.000095[x_{Mn}], \qquad (2)$$

where α_γ, x_C, and x_{Mn} are a lattice parameter (angstrom), carbon and manganese content (wt.%) in RA, accordingly [18]. Lattice parameter was found as [35]:

$$a_\gamma = \sqrt{h^2 + k^2 + l^2}\frac{\lambda}{2\sin\theta}, \qquad (3)$$
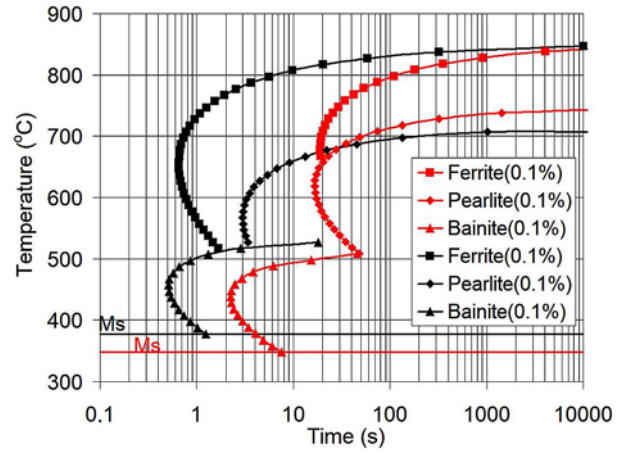

Fig. 2. TTT-diagrams for steel A (black lines) and steel B (red lines). The lines correspond to the transformation onset (0.1 vol.%) (calculated by JMatPro).

where h, k, and l are the indices of crystallographic plane of diffraction, λ is the X-ray wave length.

3. Results

3.1. Austenite transformation behavior and microstructure characterization

The chemical composition of the steel greatly affects the kinetics of austenite transformation, influencing the structure formation during heat treatment. The transformation behavior of the steels studied was evaluated using a JMatPro computer simulation. Temperature-Time-Transformation (TTT) diagrams (Fig. 2) were calculated for the austenitization temperature of 930 °C and grain size of 10 μm. As it was found earlier [36], lower temperature (900 °C) corresponds to the dual-phase (ferrite + austenite) interval in steel B. Therefore, the austenitization temperature of 930 °C was chosen for a simulation to ensure a single-phase austenitic state in both steels. According to TTTs, the upper temperatures of "austenite → ferrite" and "austenite → pearlite" transformations in steel A were 707 and 851 °C, respectively. The kinetics maximum of proeutectoid ferrite formation in steel A was attributed to 650 °C with an incubation period of less than 1 s (0.65 s). The highest rate of pearlite transformation referred to 567 °C with an incubation period of 3 s. Bainite domain was allocated below 533 °C; the highest transformation rate of bainite reaction corresponded to 457 °C with an incubation period of 0.5 s.

Alloying with Cr, Mo, and V (steel B) increased the upper temperatures of ferrite/pearlite transformations (751 and 854 °C, respectively) and decreased the upper temperature of the bainite reaction (508 °C). The temperature of the kinetics maximum of ferrite and pearlite transformations increased to 688 and 620 °C,
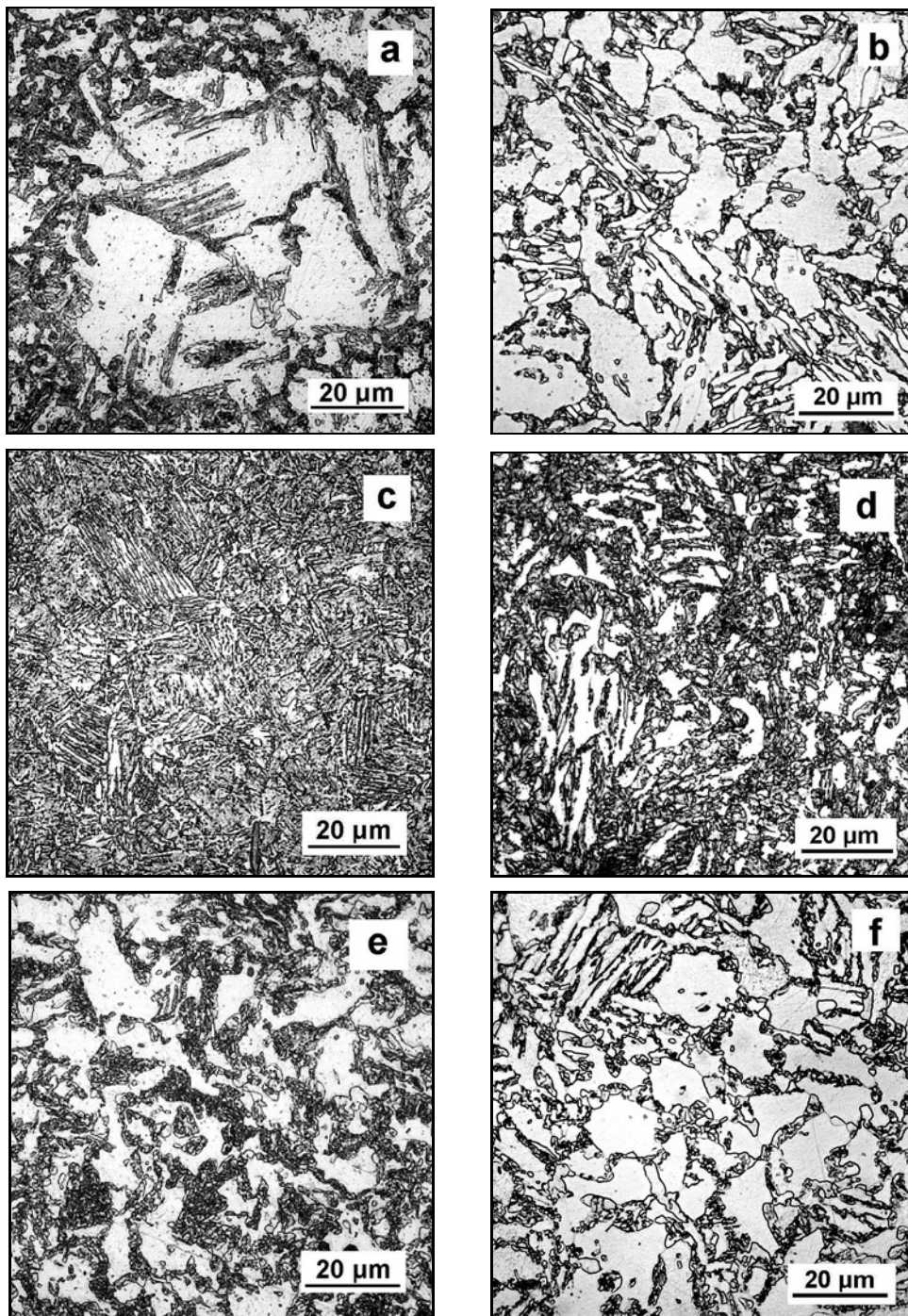
Fig. 3a–f. OM microstructure of steel A (a, c, e) and steel B (b, d, f) after bainitizing at 770-350 °C (a, b) and 900-350 °C (c, d) and after Q&P treatment at 770-200-350 °C (e, f).

respectively, while the temperature of the kinetics maximum of "austenite → bainite" transformation decreased to 438 °C. Notably, steel B performed enhanced stability of overcooled austenite at each temperature in the sub-critical range: the minimum incubation period increased by 27 times, 6 times, and 4 times for ferrite/pearlite/bainite transformations, respectively. Herewith, additional alloying increased austenite stability for ferrite/pearlite transformations to a

higher extent leading to a more pronounced allocation of the bainite domain [37, 38]. One can conclude that steel B had a higher hardenability and a higher propensity for bainite formation as compared with steel A. Moreover, steel B exhibited a lower martensite transformation start temperature (Ms = 346 °C) as compared with steel A (377 °C) due to slightly higher carbon content and additional alloying with chromium and molybdenum.
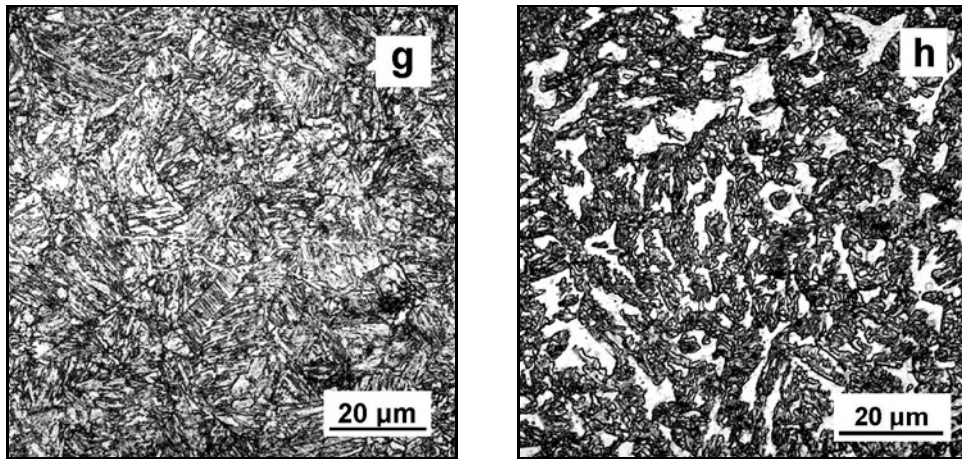
Fig. 3g,h. OM microstructure of steel A (g) and steel B (h) after bainitizing at 900-235-350 ℃ (g, h).

The OM microstructures of heat-treated steels are illustrated in Fig. 3. The bainitizing at 350 ℃ after austenitization at 770 ℃ resulted in a structure consisting of polygonal proeutectoid ferrite grains and bainite areas located mostly along the grain boundaries (Fig. 3a,b). Bainitizing from 900 ℃ significantly increased bainite volume fraction, as that steel A almost had no ferrite in the structure (Fig. 3c) while steel B still contained a minor fraction of ferrite (Fig. 3d). Almost the same OM microstructural patterns were observed in the specimens subjected to Q&P heat treatment (depending on austenitization temperatures). When comparing the bainitized specimens and Q&P treated specimens, the non-ferritic regions appeared similar, exhibiting lath morphology. The distinctive morphological features of steel structure can be observed in SEM images captured at higher magnification (Fig. 4). Bainitized specimens (Fig. 4a) performed lower bainite (the bunches of parallel ferrite plates) and MA compact islands. Q&P-treated specimens (Fig. 4b) exhibited the lath pattern being a mix of martensite and lower bainite. In both images, the ferrite grains are presented as well.

X-ray diffraction was used to determine the steel phase status. XRD patterns for both steels are shown in Fig. 5. The distinctive feature of these patterns was intensive peaks belonging to alpha-Fe (bcc lattice). Also, XRD patterns included the weak peaks (200) and (220) of γ-Fe (fcc lattice); the peak (111)fcc peak superimposed on (111)bcc while the peak (311)fcc was not revealed at all. The weakness of the γ-Fe peaks indicated the minor presence of retained austenite in the specimens' structure. The values of retained austenite volume fraction are presented in Table 2. For steel A, VF_{RA} was calculated for the bainitized specimen (900-350) and for the Q&P-treated specimen (900-235-350) to be 6.0–6.3 vol.%, while the measurements of VF_{RA} for other regimes were not reliable because of very weak austenite peaks. In contrast, for steel B,
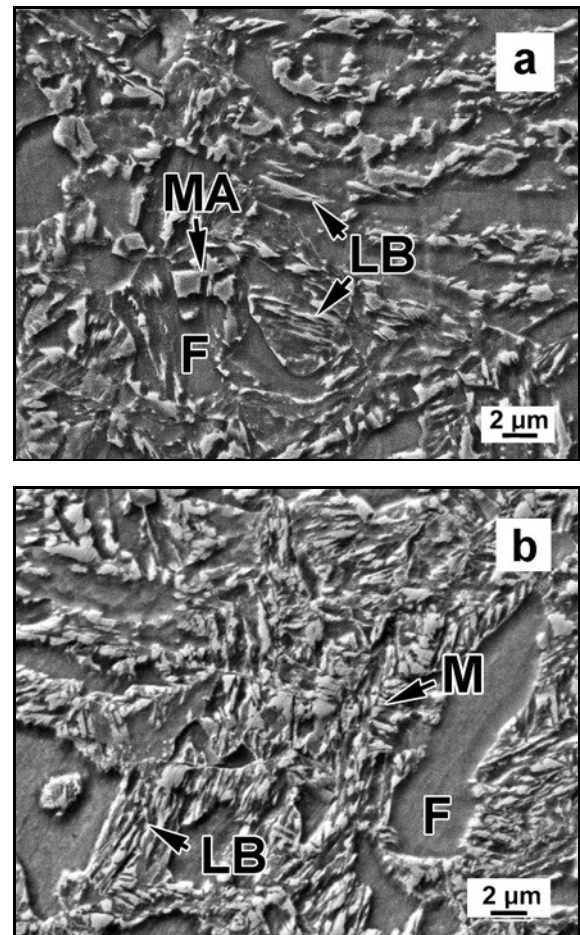

Fig. 4. SEM microstructure of steel B after (a) bainitizing (900-350 ℃) and (b) Q&P treatment (900-235-350 ℃) (F, LB, M, MA – ferrite, lower bainite, martensite, martensite-austenite island, accordingly).

VF_{RA} value was calculated for all the regimes varying from 4.4–5.5 vol.% (for bainitizing) to 8.1–8.7 vol.%

T a b l e 2. Volume fraction/carbon content of retained austenite in steels after heat treatment

Heat treatment mode	Steel A		Steel B	
	RA volume fraction (vol.%)	RA carbon content (wt.%)	RA volume fraction (vol.%)	RA carbon content (wt.%)
Bainitizing (700-350)	not detected	not detected	4.4	0.80
Bainitizing (900-350)	6.0	0.57	5.5	0.78
Q&P (770-200-350)	not detected	not detected	8.0	0.85
Q&P (900-235-350)	6.3	0.69	8.7	0.93
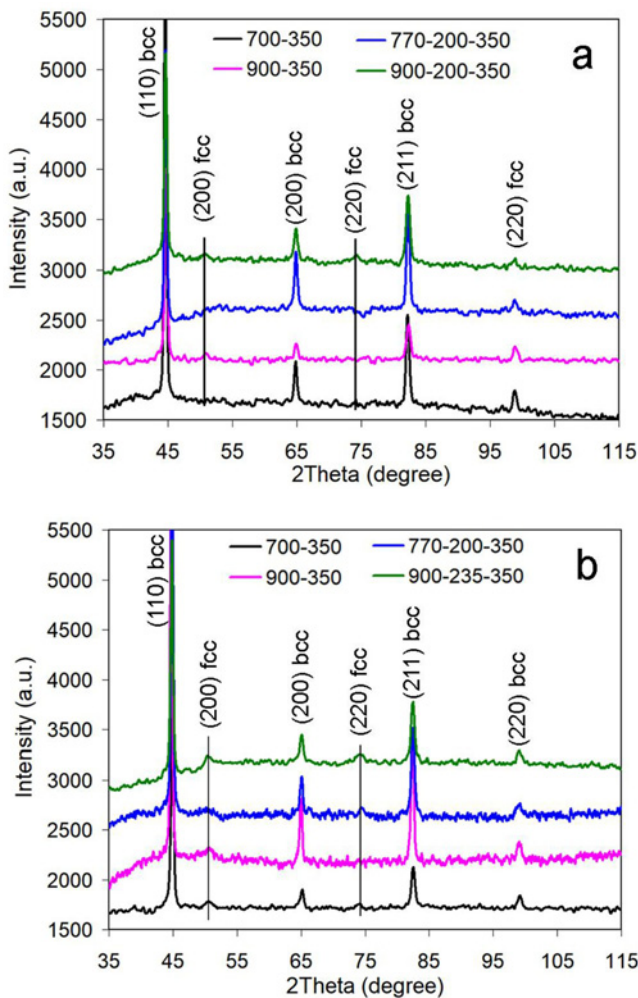
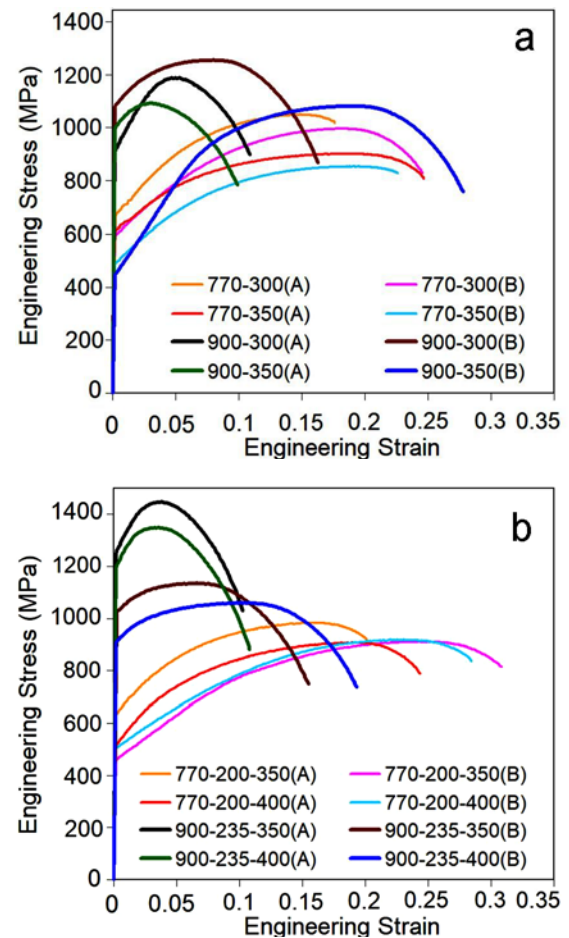Fig. 5. XRD patterns for (a) steel A and (b) steel B after bainitizing and at Q&P treatment.

Fig. 6. Engineering Strain – Engineering Stress curves for (a) bainitized specimens and (b) Q&P-treated specimens (A and B – steel designation).

(for Q&P treatment). The carbon content in RA was measured as 0.78–0.93 wt.% for steel B, which was 3.5–5 times to nominal carbon content in the steel. The specimens of steel A had lower content in retained austenite (0.57–0.69 wt.%).

3.2. Mechanical properties evaluation

The tensile test results were presented as engineer-ing strain-stress curves shown in Fig. 6. As seen, in any case, the experimental steels performed continuous yielding with a neck formation. The specimens austenized at 900 ℃ exhibited a more pronounced load decrease under the necking, meaning the higher area reduction before fracture as compared with austeniti-zation at 770 ℃.

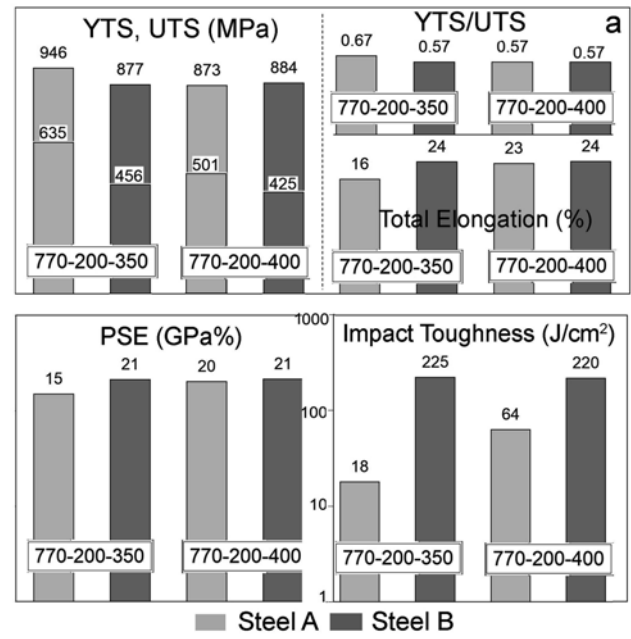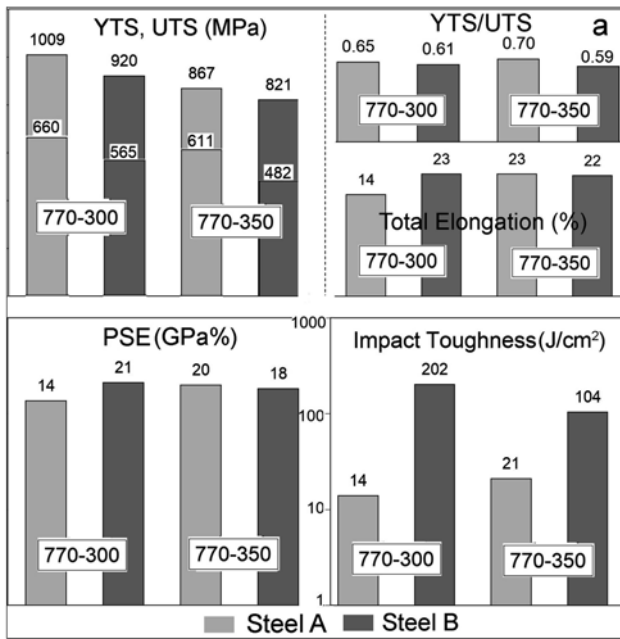The mechanical properties of bainitized speci-mens are presented in Fig. 7 to be given together

Fig. 7. Mechanical properties of bainitized steels. Austenitization at (a) 770 ℃ and (b) 900 ℃.

Fig. 8. Mechanical properties of Q&P-treated steels. Austenitization at (a) 770 ℃ and (b) 900 ℃.

for both steels for easier comparison. As seen in Fig. 7a, after austenitization at 770 ℃ and bainitizing at $t_B = 350$ ℃, the steel A exhibited a yield tensile strength (YTS, determined under the strain of 0.2 %) of 611 MPa and ultimate tensile strength (UTS) of 867 MPa. Bainitizing treatment at 300 ℃ increased YTS and UTS to 660 MPa and 1009 MPa accordingly. Steel B exhibited slightly lower strength characteristics (YTS/UTS): 482 and 821 MPa at $t_B = 350$ ℃ and 562 and 920 MPa at $t_B = 300$ ℃. Steel A showed

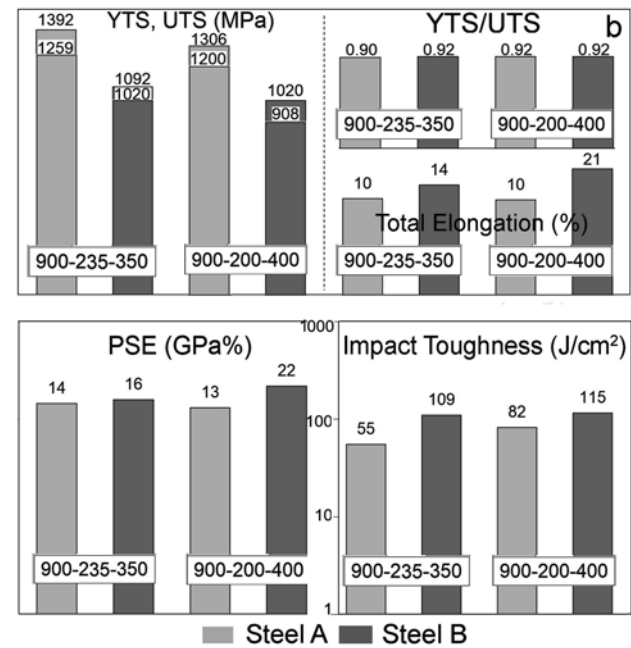a higher YTS/UTS ratio for both bainitizing temperatures. Under $t_B = 300$ ℃, steel B was more ductile at having total elongation (TE) of 23 % against 14 % of steel A. Under $t_B = 350$ ℃, both steels had similar TE values of about 22–23 %. Using the data on UTS and TE, the values of the product of strength and elongation (PSE) were calculated. The highest PSE values were attributed to steel B (21 GPa·%) at $t_B = 300$ ℃ and to steel A (20 GPa·%) at $t_B = 350$ ℃. The most significant difference in properties corresponded

to impact toughness (KCV$_{20°C}$): steel B showed 104–202 J cm^{-2}, which was a magnitude higher as compared with steel A (14–21 J cm^{-2}). Thus, after bainitizing from 770 ℃, steel A performed some advantage in strength indicators, but it was much inferior in terms of impact toughness.

The bainitizing treatment after heating at 900 ℃ resulted in a total increase in YTS and UTS values (Fig. 7b) while yield tensile strength increased to more extent; thus, the YTS/UTS ratios also increased as compared to $t_A = 770$ ℃. The steels exhibited the same strength level with some advantage of steel B under $t_B = 300$ ℃ and steel A under $t_B = 350$ ℃. In contrast, steel B was much more ductile (by 1.5–2 times) for any bainitizing temperature: despite strength increase, the TE values of steel B were also increased to 18 % ($t_B = 300$ ℃) and 23 % ($t_B = 350$ ℃). Accordingly, steel B showed itself as a more ductile and tougher material with advanced properties combination performing PSE of 22–24 GPa·% and twice higher impact toughness.

Mechanical properties of steels subjected to Q&P are depicted in Fig. 8. After treatment from 770 ℃, both steels mostly had similar YTS, UTS, TE, PSE, and YTS/HTS. The exception referred to $t_P = 350$ ℃ when steel A showed higher YTS and UTS (by 179 and 69 MPa) and lower TE (by 8 %) and PSE (by 5 GPa·%) values. As previously noted for bainitizing, Q&P-treated steel B exhibited a significant advantage in impact toughness, which was 12.5 times at $t_P = 350$ ℃ and 3.4 times at $t_P = 350$ ℃. Q&P-treatment from 900 ℃ led to a significant increase in strength with a corresponding decrease in ductility/impact toughness. In this case, steel A was stronger by 250–300 MPa but less ductile (by 4–11 %) than steel B. Steel B also showed an improved impact toughness; however, its advantage was lesser than that of $t_Q = 770$ ℃. The highest PSE value among all Q&P-treated specimens (22 GPa·%) was attributed to steel B after the regime of 900-235-400.

4. Discussion

The effect of alloying elements can be derived from the results shown in Fig. 7 where the correlations of the mechanical properties are displayed. As seen in Figs. 9a,b, more alloyed steel B performed better strength/ductility after both heat treatments. Specifically, steel B had a higher total elongation at the same UTS (blue curve) as compared to steel A (red curve); this behavior refers to a UTS range of up to 1200 MPa (bainitizing) and up to 1000 MPa (Q&P). The trends of strength increase and ductility decrease with a rising austenitization temperature from 770 to 900 ℃ are seen. Bainitized steel B presented higher TE values in a wide UTS range (800–1200 MPa) (Fig. 9a). Further-

more, steel B exhibited an improved "UTS/Impact Toughness" combination (Figs. 9c,d) that was more evident for UTS = 800–1000 MPa (bainitizing) and UTS = 850–1100 MPa (Q&P). As to impact toughness, two different trends were observed: steel B had higher KCV$_{20°C}$ values after heat treatment from $t_A = 770$ ℃ while steel A showed the better KCV$_{20°C}$ values after austenitizing at 900 ℃. Finally, steel B had an indisputable (by 1.5–2.0 times) advantage in PSE value compared to steel A at the same UTS value (Fig. 9e), meaning an enhanced ability for reliable performance under exploitation conditions.

After heat treatment from $t_A = 900$ ℃, steel B showed lower strength than that of steel A. This was ascribed to the presence of some proeutectoid ferrite in steel B while steel A contained no ferrite. According to the JMatPro simulation, steel B had higher upper temperatures of pearlite/ferrite transformation; thus, it should contain a higher amount of ferrite at any temperature belonging to an intercritical range. Accordingly, the temperature of 900 ℃ belonged to a single-phase (austenite) domain for steel A while it was within the dual-phase interval (ferrite + austenite) for steel B, causing proeutectoid ferrite presence in steel B structure.

The improved complex of mechanical properties of steel B refers to its higher alloying level that enables the formation of a multiphase heterogeneous microstructure with an increased amount of retained austenite. Presumably, a higher (by 0.29 wt.%) silicon content contributes to more complete inhibition of cementite precipitation during bainitizing (or partitioning) holding, thus increasing carbon content in austenite. Moreover, the presence of 0.55 wt.% Cr and 0.20 wt.% Mo should lower the martensite temperature Ms. According to Sverdlin-Ness's equation [39], each percentage of Cr and Mo decreases Ms by 30 and 20 ℃, respectively. Lowering the martensite point affects a driving force of martensite transformation while Cr/Mo increases austenite strength through a solute strengthening mechanism [27], leading to austenite retention. Considering the Cr and Mo concentration in steel B, the decrease in Ms was calculated as 20.5 K. A corresponding increase in a retained austenite amount (in the case of Q&P treatment) can be derived from a Koistinen-Marburger equation (Eq. 4):

$$f_{RA} = (1 - (1 - \exp(-a_m(Ms - t_Q)))). \qquad (4)$$

Taking $a_m = 0.008$ [40], $t_Q = 20$ ℃, Ms decrease = 20.5 K, a Cr/Mo-affected increase in retained austenite was calculated as 2.8 vol.%. An increase in RA volume fraction also can be caused by austenite carbon enrichment due to higher silicon content in steel B. According to Sverdlin-Ness's equation, an increase in carbon concentration by 0.1 wt.% could result in a Ms
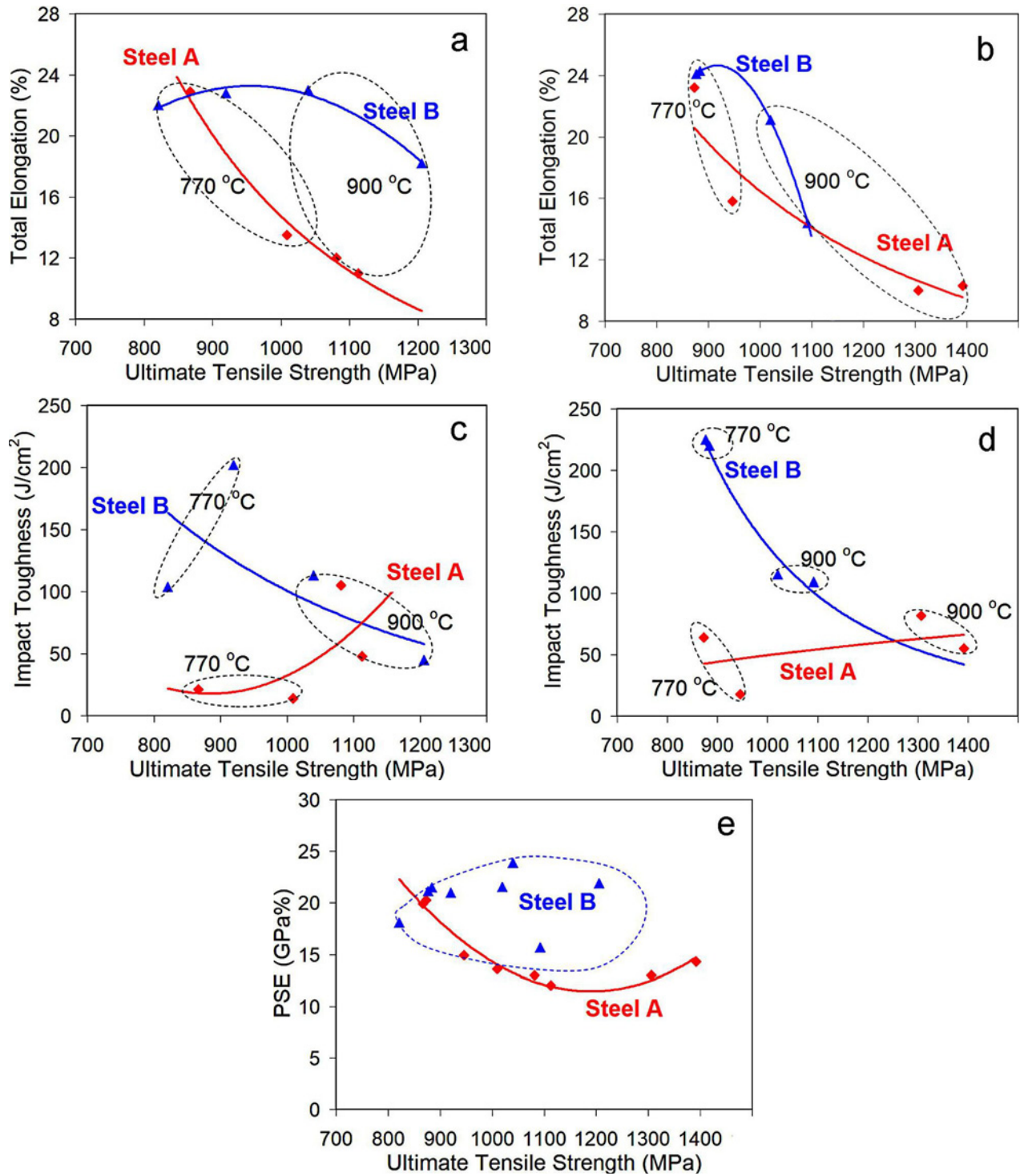
Fig. 9. The properties correlations: "UTS-TE" for (a) bainitizing and (b) Q&P treatment; "UTS-Impact Toughness" for (c) bainitizing and (d) Q&P treatment; (e) "UTS-PSE" for both heat treatment schemes.

decrease of 32 K, meaning a 4.6 vol.% increase in RA volume fraction.

These theoretical considerations were supported experimentally by the XRD study (Table 2), which presented the higher amount of retained austenite in steel B irrespectively of heat-treatment mode (Table 2). As follows from Fig. 9, the higher VF_{RA} was beneficial for ductility and impact toughness of steel B. A positive effect of retained austenite on impact toughness was most evident under the austenitization at 770 °C: in this case, steel B had a significant advantage over steel A (4–8 times under bainitizing and 5–7 times under Q&P treatment). Notably, under $t_A = $ 770 °C, steel A had much lower $KCV_{20°C}$ values de-
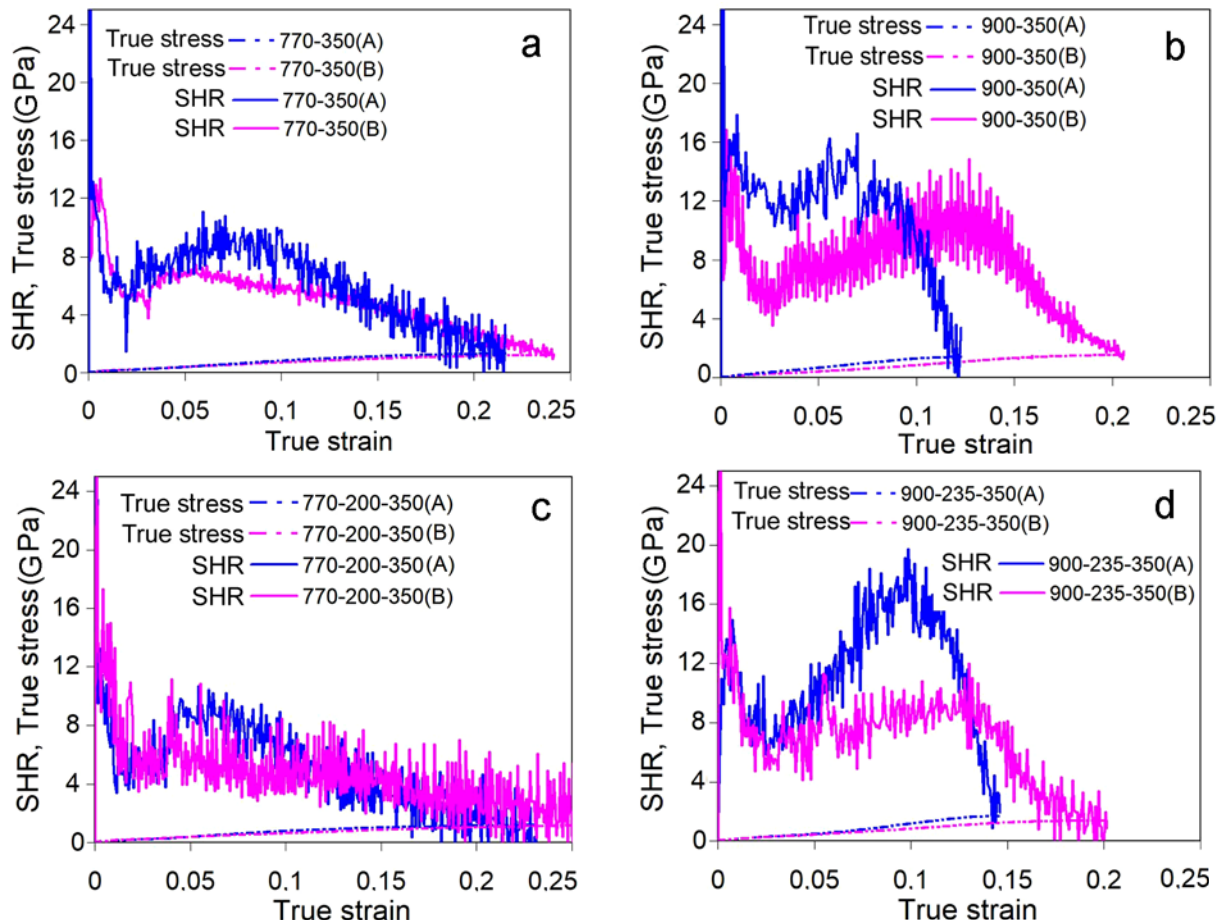
Fig. 10. Strain hardening rate (SHR) and true stress curves for (a, b) bainitizing and (c, d) Q&P treatment.

spite the presence of an increased amount of soft ferrite in the structure. This behavior of steel A refers to carbon partitioning from ferrite into austenite under heating at 770 °C, which led to 0.4 wt.% C content in austenite. Carbon-rich austenite transformed into high-carbon (brittle) martensite under Q&P treatment or discharged into carbide precipitation during bainitizing (partitioning) holding, causing high brittleness of steel. In contrast, heat treatment with $t_A =$ 900 °C resulted in less carbon content in austenite before bainitizing/quenching that presumably prevented carbide precipitation from austenite. Thus carbon was accumulated in austenite resulting in the increase of RA volume fraction (as seen from XRD patterns) with an eventual increase in the impact toughness.

As follows from Table 2, Q&P treatment led to a slightly higher amount of retained austenite as compared with bainitizing treatment. The possible reason is the mechanical stabilization of austenite by martensite, which appeared in the structure before the partitioning stage. Hard martensite laths constrained the austenite expansion caused by fcc→bcc lattice alteration [25], inhibiting bainite transformation at partitioning holding.

The different impact toughness of the steels can also be explained regarding the stability of retained austenite to strain-induced martensite transformation (SIMT). This factor is crucial for the ductility/impact toughness of multiphase steel, which contains the hard phase constituents (as martensite or lower bainite) [17]. Impact toughness is especially sensitive to the phase properties and RA amount, serving as a brittle fracture preventer. The propensity of RA to SIMT is controlled by Md temperature, which mostly depends on carbon content in austenite [5]. An increase in carbon content decreases Md temperature [41], thus stabilizing austenite. Stabilized austenite is expected to perform slow kinetics of SIMT with extended TRIP-effect, thus preventing early embrittlement caused by rapid formation of deformation-induced martensite [41]. Since the steels A and B differed by carbon content in RA, they should also differ in TRIP kinetics affecting the mechanical properties.

The RA metastability under tensile loading was analyzed using the curves of strain hardening rate (SHR) derived from the tensile curves as SHR = $d\sigma/d\varepsilon$, where σ and ε are true stress and true strain accordingly. SHR curves for both steels are shown in Fig. 10.

Early strain stage (up to $\varepsilon \approx 0.025$) was character-

ized by SHR drop connected with cumulative interactions of moving dislocations and blocking the close-packed plains along which the dislocations glide [41]. Then the SHR increased, manifesting the next hardening stage caused by TRIP-effect [42]. As seen in all cases, the SHR curve for steel A reached higher maximal values indicating a higher SIMT rate. The difference in maximal SHR value was bigger for the specimens treated from 900 °C (Figs. 8b,d), which can be explained by the absence of proeutectoid ferrite in steel A. Since retained austenite is the only ductile phase in steel A, then plastic deformation started exactly in austenite at a lower strain than that of steel B containing proeutectoid ferrite. Also, the second phase of strain hardening in steel B lasted for a bigger strain meaning more slow kinetics of SIMT. This behavior resulted in delaying the plastic instability state, which is the start of neck formation. According to [43], the criterion for plastic instability is $\mathrm{d}\sigma/\mathrm{d}\varepsilon = \sigma$ found in the intersection of the SHR curve and the true stress-strain curve. As seen in Fig. 10, steel B exhibited plastic instability at higher strain for any heat treatment mode, which is important for increasing uniform elongation. This allowed us to assume that steel B possessed retained austenite with appropriate stability and slower SIMT kinetic, contributing to a higher strength/ductility/toughness combination. In contrast, retained austenite in steel A transformed faster, accelerating the occurrence of plastic instability. The reasons for different SIMT behavior of the steels are higher carbon enrichment of RA in steel B (due to higher Si content) and the effect of Cr and Mo, which mechanically stabilized austenite due to solid solution hardening [29].

Another possible reason for the enhanced ductility/toughness of steel B was adding vanadium (0.11 wt.%). Vanadium is a strong nitride-forming element [44] known to absorb nitrogen, thus reducing N content in a crystalline lattice. This increases the mobility of a gliding dislocation in a crack tip area, thus inhibiting crack propagation [45].

5. Conclusions

Based on the results obtained, some major conclusions were drawn from this research. Two TRIP-assisted steels (Mn-Si-Nb and Mn-Si-Cr-Mo-V-Nb) containing 0.2 wt.% C were comparatively studied in order to evaluate the effect of chemical composition on austenite transformation kinetic and tensile/impact behavior after bainitizing treatment and Q&P treatment. It was found that adding 0.55 wt.% Cr, 0.2 wt.% Mo, and 0.11 wt.% V into Mn-Si-Nb steel led to increasing austenite stability in pearlite and bainite temperature domains by 6 and 4 times, respectively, insulating the bainite transformation domain below 508 °C. The steels performed UTS in a range of 821–1392 MPa and total elongation in a range of 12–24 %, depending on the heat treatment regime. Additional alloying resulted in an improvement of "Strength/Ductility/Impact Toughness" combinations where a maximum PSE index (24 GPa·%) was obtained in steel B after bainitizing treatment, whereas the highest $KCV_{20\,°C}$ values (220–225 J cm^{-2}) were gained by Q&P treatment. Improved mechanical behavior of additionally-alloyed steel was due to increased amount of retained austenite and a slower kinetic of TRIP-effect caused by appropriate stability of retained austenite to strain-induced martensite transformation.

References

[1] E. A. Da Silva, L. F. V. Malerba Fernandes, J. W. De Jesus Silva, R. B. Ribeiro, M. A. Dos Santos Pereira, Comparison between an advanced high-strength steel and a high-strength steel due to the spring back effect, IOSR Journal of Mechanical and Civil Engineering 13 (2016) 21–27. doi:10.9790/1684-1305012127

[2] Z. M. Rykavets, J. Bouquerel, J.-B. Vogt, Z. A. Duriagina, V. V. Kulyk, T. L. Tepla, L. I. Bohun, T. M. Kovbasyuk, Investigation of the microstructure and properties of TRIP 800 steel subjected to low-cycle fatigue, Usp. Fiz. Met. 20 (2019) 620–633. doi:10.15407/ufm.20.04.620

[3] M. Soleimani, A. Kalhor, H. Mirzadeh, Transformation-induced plasticity (TRIP) in advanced steels: A review, Mater. Sci. Eng. A 795 (2020) 140023. doi:10.1016/j.msea.2020.140023

[4] V. Kukhar, O. Kurpe, E. Klimov, E. Balalayeva, V. Dragobetskii, Improvement of the method for calculating the metal temperature loss on a coilbox unit at the rolling on hot strip mills, International Journal of Engineering and Technology (UAE) 7 (2018) 35–39. doi:10.14419/ijet.v7i4.3.19548

[5] W. Bleck, X. Guo, Y. Ma, The TRIP effect and its application in cold formable sheet steels, Steel Res. Int. 88 (2019) 1700218. doi:10.1002/srin.201700218

[6] C. Lesch, N. Kwiaton, F. B. Klose, Advanced high strength steels (AHSS) for automotive applications − tailored properties by smart microstructural adjustments, Steel Res. Int. 88 (2017) 1700210. doi:10.1002/srin.201700210

[7] T. Taylor, K. Kim, J. Zhang, D. Penney, J. Yanagimoto, TRIP assisted press hardened steel by the anisothermal bainitic ferrite transformation, J. Mater. Process. Technol. 289 (2021) 116950. doi:10.1016/j.jmatprotec.2020.116950

[8] N. Fonstein, Advanced High Strength Sheet Steels: Physical Metallurgy, Design, Processing, and Properties. Springer International Publishing, Switzerland, 2015. ISBN: 978-3-319-19164-5

[9] X. Gu, Y. Xu, F. Peng, R. D. K. Misra, Y. Wang, Role of martensite/austenite constituents in novel ultra-high strength TRIP-assisted steels subjected to non-isothermal annealing, Mater. Sci. Eng. A 754 (2019) 318–329. doi:10.1016/j.msea.2019.03.070

[10] B. L. Ennis, E. Jimenez-Melero, E. H. Atzem, M. Krugl, M. A. Azeem, D. Rowley, D. Daisenberg-ere, D. N. Hanlon, P. D. Lee, Metastable austenite driven work-hardening behaviour in a TRIP-assisted dual phase steel, Int. J. Plast. 88 (2017) 126–139. doi:10.1016/j.ijplas.2016.10.005

[11] A. Eres-Castellanos, C. Garcia-Mateo, F. G. Caballero, Future trends on displacive stress and strain induced transformations in steels, Metals 11 (2021) 299. doi:10.3390/met11020299

[12] Z. J. Xie, S. F. Yuan, W. H. Zhou, J. R. Yang, H. Guo, C. J. Shang, Stabilization of retained austenite by the two-step inter-critical heat treatment and its effect on the toughness of a low alloyed steel, Mater. Des. 59 (2014) 193–198. doi:10.1016/j.matdes.2014.02.035

[13] X. Tan, H. He, W. Lu, L. Yang, B. Tang, J. Yan, Y. Xu, D. Wu, Effect of matrix structures on TRIP effect and mechanical properties of low-C low-Si Al-added hot-rolled TRIP steels, Mater. Sci. Eng. A 771 (2020) 138629. doi:10.1016/j.msea.2019.138629

[14] O. Hesse, J. Merker, M. Brykov, V. Efremenko, On the strength of low-alloy steels with increased carbon content against abrasive wear, Tribol. Schmierungstech 60 (2013) 37–43. (in German)

[15] A. D. Koval, V. G. Efremenko, M. N. Brykov, M. I. Andrushchenko, R. A. Kulikovskii, A. V. Efremenko, Principles for developing grinding media with increased wear resistance. Part 1. Abrasive wear resistance of iron-based alloys, Journal of Friction and Wear 33 (2012) 39–46. doi:10.3103/S1068366612010072

[16] B. Zhang, L. X. Du, Y. Dong, D. X. Han, H. Y. Wu, F. H. Lu, R. D. K. Misra, Structure-property relationship in novel low carbon hot-rolled TRIP steels via thermo-mechanical controlled processing and coiling, Mater. Sci. Eng. A 771 (2020) 138643. doi:10.1016/j.msea.2019.138643

[17] L. S. Malinov, I. E. Malysheva, E. S. Klimov, V. V. Kukhar, E. Balalayeva, Effect of particular combinations of quenching, tempering and carburization on abrasive wear of low-carbon manganese steels with metastable austenite, Mater. Sci. Forum 945 (2019) 574–578. doi:10.4028/www.scientific.net/MSF.945.574

[18] A. Karimi, S. Kheirandish, M. Mahmoudiniya, Effect of bainite volume fraction on mechanical properties of a ferrite-bainite-martensite steel, Kovove Mater. 55 (2017) 175–182. doi:10.4149/km2017_3_175

[19] V. I. Zurnadzhy, V. G. Efremenko, I. Petryshynets, K. Shimizu, M. N. Brykov, I. V. Kushchenko, V. V. Kudin, Mechanical properties of carbide-free lower bainite in complex-alloyed constructional steel: Effect of bainitizing treatment parameters, Kovove Mater. 58 (2020) 129–140. doi:10.4149/km_2020_2_129

[20] E. A. Ariza, A. S. Nishikawa, H. Goldenstein, A. P. Tschiptschin, Characterization and methodology for calculating the mechanical properties of a TRIP-steel submitted to hot stamping and quenching and partitioning (Q&P), Mater. Sci. Eng. A 671 (2016) 54–69. doi:10.1016/j.msea.2016.06.038

[21] V. I. Zurnadzhy, V. G. Efremenko, K. M. Wu, A. Yu. Azarkhov, Yu. G. Chabak, V. L. Greshta, O. B. Isayev, M. V. Pomazkov, Effects of stress relief tempering on microstructure and tensile/impact behavior of quenched and partitioned commercial spring steel, Mater. Sci. Eng. A 745 (2019) 307–318. doi:10.1016/j.msea.2018.12.106

[22] V. Efremenko, K. Shimizu, T. Pastukhova, Yu. Chabak, M. Brykov, K. Kusumoto, A. Efremenko, Three-body abrasive wear behaviour of metastable spheroidal carbide cast irons with different chromium contents, Int. J. Mater. Res. 109 (2018) 147–156. doi:10.3139/146.111583

[23] A. F. Santacruz-Londono, O. Rios-Diez, J. A. Jiménez, C. Garcia-Mateo, R. Aristizábal-Sierra, Microstructural and mechanical characterization of a nanostructured bainitic cast steel, Metals 10 (2020) 612. doi:10.3390/met10050612

[24] S. B. Singh, H. K. D. H. Bhadeshia, Estimation of bainite plate-thickness in low-alloy steels, Mater. Sci. Eng. A 245 (1998) 72–79. doi:10.1016/S0921-5093(97)00701-6

[25] C. Garcia-Mateo, G. Paul, M. C. Somani, D. A. Porter, L. Bracke, A. Latz, C. G. De Andres, F. G. Caballero, Transferring nanoscale bainite concept to lower C contents: A perspective, Metals 7 (2017) 159. doi:10.3390/met7050159

[26] V. I. Zurnadzhy, V. G. Efremenko, K. M. Wu, I. Petryshynets, K. Shimizu, A. M. Zusin, M. N. Brykov, V. A. Andilakhai, Tailoring strength/ductility combination in 2.5 wt.% Si-alloyed middle carbon steel produced by the two-step Q-P treatment with a prolonged partitioning stage, Mater. Sci. Eng. A 791 (2020) 139721. doi:10.1016/j.msea.2020.139721

[27] G. Gao, B. Gao, X. Gui, J. Hu, J. He, Z. Tan, B. Baia, Correlation between microstructure and yield strength of as-quenched and Q&P steels with different carbon content (0.06–0.42 wt.% C), Mater. Sci. Eng. A 753 (2019) 1–10. doi:10.1016/j.msea.2019.03.018

[28] M. Ollat, J. P. Masse, M. Bouzat, Influence of partitioning on mechanical behavior of Q&P steels, Mater. Sci. Eng. A 661 (2016) 79–86. doi:10.1016/j.msea.2016.02.071

[29] C. Garcia-Mateo, T. Sourmail, F. G. Caballero, V. Smanio, M. Kuntz, C. Ziegler, A. Leiro, E. Vuorinen, R. Elvira, T. Teeri, Nanostructured steel industrialisation: plausible reality, Mater. Sci. Technol. 30 (2014) 1071–1078. doi:10.1179/1743284713Y.0000000428

[30] Y. J. Li, D. Chen, D. Liu, J. Kang, G. Yuan, Q. J. Mao, R. D. K. Misra, G. D. Wang, Combined thermo-mechanical controlled processing and dynamic carbon partitioning of low carbon Si/Al-Mn steels, Mater. Sci. Eng. A 732 (2018) 298–310. doi:10.1016/j.msea.2018.07.021

[31] Z. Zeng, K. M. Reddy, S. Song, J. Wang, L. Wang, X. Wang, Microstructure and mechanical properties of Nb and Ti microalloyed lightweight δ-TRIP steel,

Mater. Charact. 164 (2020) 110324. doi:10.1016/j.matchar.2020.110324

[32] A. G. Kostryzhev, O. O. Marenych, C. R. Killmore, E. V. Pereloma, Strengthening mechanisms in thermomechanically processed NbTi-microalloyed steel, Metall. Mater. Trans. A 46 (2015) 3470–3480. doi:10.1007/s11661-015-2969-2

[33] A. J. Clarke, J. G. Speer, M. K. Miller, R. E. Hackenberg, D. V. Edmonds, D. K. Matlock, E. De Moor, Carbon partitioning to austenite from martensite or bainite during the quench and partition (Q&P) process: A critical assessment, Acta Mater. 56 (2008) 16–22. doi:10.1016/j.actamat.2007.08.051

[34] S. Jing, H. Yu, Microstructure development and mechanical properties of quenching and partitioning (Q&P) steel and an incorporation of hot-dipping galvanization during Q&P process, Mater. Sci. Eng. A 586 (2013) 100–107. doi:10.1016/j.msea.2013.08.021

[35] N. H. Van Dijk, A. M. Butt, L. Zhao, Thermal stability of retained austenite in TRIP steels studied by synchrotron X-ray diffraction during cooling, Acta Mater. 53 (2005) 5439–5447. doi:10.1016/j.actamat.2005.08.017

[36] R. Kussa, I. Kushchenko, V. Andilakhai, I. Petryshynets, V. Efremenko, V. Zurnadzhy, Austenite transformation behavior and mechanical properties of constructional V, Nb-alloyed TRIP-assisted steel, Key Engineering Materials 864 (2020) 241–249. doi:10.4028/www.scientific.net/KEM.864.241

[37] B. Efremenko, A. Belik, Y. Chabak, H. Halfa, Simulation of structure formation in the Fe-C-Cr-Ni-Si surfacing materials, East.-Eur. J. Enterp. Technol. 2 (2018) 33–38. doi:10.15587/1729-4061.2018.124129

[38] S. I. Ryabtsev, V. A. Polonskyy, O. V. Sukhova, Effect of scandium on the structure and corrosion properties of vapor-deposited nanostructured quasicrystalline Al-Cu-Fe films, Powder Metall. Met. Ceram. 58 (2020) 567–575. doi:10.1007/s11106-020-00111-2

[39] A. V. Sverdlin, A. R. Ness, The Effects of Alloying Elements on the Heat Treatment of Steel, in: G. E. Totten, M. A. H. Howes (Eds.), Heat Treatment Handbook, Marcel Dekker, New York 1997, pp. 45–91. ISBN: 9780824727413

[40] M. G. Mendiratta, G. Krauss, Development of martensitic microstructure and microcracking in an Fe-1.86C alloy, Metall. Mater. Trans. B 3 (1972) 1755–1760. doi:10.1007/BF02642557

[41] D. T. Lewis, J. G. Speer, D. K. Matlock, M. C. Mataya, Influence of composition variation on deformation induced martensite formation in type 304 stainless steel, 41st MWSP Conference Proceedings ISS 37 (1999) 343–351.

[41] B. Zhang, L. X. Du, Y. Dong, D. X. Han, H. Y. Wu, F. H. Lu, R. D. K. Misra, Structure-property relationship in novel low carbon hot-rolled TRIP steels via thermo-mechanical controlled processing and coiling, Mater. Sci. Eng. A 771 (2020) 138643. doi:10.1016/j.msea.2019.138643

[42] M. Zhang, W. Cao, H. Dong, J. Zhu, Element partitioning effect on microstructure and mechanical property of the micro-laminated Fe-Mn-Al-C dual phase steel, Mater. Sci. Eng. A 654 (2016) 193–202. doi:10.1016/j.msea.2015.12.029

[43] R. Song, D. Ponge, D. Raabe, Mechanical properties of an ultrafine grained C-Mn steel processed by warm deformation and annealing, Acta Mater. 53 (2005) 4881–4892. doi:10.1016/j.actamat.2005.07.009

[44] T. Steiner, E. J. Mittemeijer, Alloying element nitride development in ferritic Fe-based materials upon nitriding: A review, J. Mater. Eng. Perform. 25 (2016) 2091–2102. doi:10.1007/s11665-016-2048-x

[45] O. P. Ostash, V. V. Kulyk, T. M. Lenkovskiy, Z. A. Duriagina, V. V. Vira, T. L. Tepla, Relationships between the fatigue crack growth resistance characteristics of a steel and the tread surface damage of railway wheel, Archives of Materials Science and Engineering 90 (2018) 49–55. doi:10.5604/01.3001.0012.0662